PCCP

Accepted Manuscript

ROYAL SOCIETY OF CHEMISTRY

www.rsc.org/pccp

Near-band-edge exciton polarization change in ZnO nanowires†

Zaiping Zeng,[a] Alexia Petoni,[a] Christos S. Garoufalis,[a] Sotirios Baskoutas*[a] and Gabriel Bester‡[b]

Using the atomistic pseudopotential method complemented by configuration interaction calculations, we have studied the electronic and optical properties of ZnO nanowires (NWs) in the presence of quantum confinement effects. Our results indicate that the near-band-edge exciton experiences a crossover from an in-plane polarized A-exciton (for D $\geq$ 3 nm) to an out-of-plane polarized C-exciton (for D $<$ 3 nm) due to quantum confinement. This transition leads to a non-monotonic variation of Stokes shift, exhibiting a maximum value around the critical diameter of 3 nm. The observed behavior is analyzed by a stepwise inclusion of correlation effects, leading to a comprehensive description of the excitonic fine structure.

1 Introduction

Zinc oxide (ZnO) nanowires (NWs) have attracted considerable attention as promising candidates for device applications. The wide direct band gap (3.445 eV) and large exciton binding energy (60 meV) of bulk ZnO make them one of the most remarkable optoelectronic materials for nanoscale device applications, such as ultraviolet (UV) lasers[1,2], light-emitting diodes[3] (LEDs), field-effect transistors (FETs)[4,5], and UV photodetectors[6,7]. Their high surface-to-volume ratio and high density of surface states promote the development of a new generation of chemical and biological gas sensors with high sensitivity and fast response[8,9]. Piezoelectric nanogenerators based on ZnO NWs for self-powered systems have also been reported[10,11]. Experimental fabrication of this type of nanostructures has been successfully achieved by using different synthesis methods, such as vapor trapping chemical vapor deposition[4], thermal evaporation[12], chemical synthesis by vapour phase transport[13], vapor–liquid–solid method[14], to mention only a few. However, the vast majority of the fabricated NWs are so large in diameter (e.g., $>$ 15 nm which is more than 10 times of the exciton Bohr radius of bulk ZnO ($\approx$1.4 nm)) that the quantum confinement effects remain absent. A clear picture of the quantum confinement effects on the electronic and optical properties of ZnO NWs remains unknown.

Due to the specific features of wurtzite ZnO, such as anisotropy of the valence band, as well as the small dielectric constant and strong electron-hole Coulomb interaction, a simple one-band effective mass model[15] is not able to deliver predictive results. The incorporation of many-body effects in an effective mass model to probe large nanostructures has been recently achieved[16,17]. Density functional theory (DFT) calculations have been employed to study the piezoelectricity and the band structure[18], the charged states and the band gap in ZnO NWs (or doped ZnO NWs)[19]. This type of calculations are restricted to nonpassivated, small-diameter (e.g., $<$ 3 nm) NWs. Moreover, since in DFT the bulk ZnO band gaps are significantly underestimated (e.g., $\sim$0.63 eV [Ref. 18] by local density approximations (LDA or GGA) (82% underestimated in comparison to the well-known experimental value 3.445 eV), the quantum confinement effects on the electronic and optical properties of ZnO NWs are often not well described.

In this contribution, we study the electronic and optical properties of ZnO NWs with diameters up to 6 nm, covering the intermediate and weak confinement regimes. The calculations are performed via the empirical pseudopotential method, using recently derived and well-tested ZnO pseudopotentials from Ref. 20, and the excitonic effects are considered by using the configuration interaction approach[21]. This method has been shown to describe very well the excitonic properties in wurtzite CdSe quantum dots (QDs)[22], and very recently in ZnO QDs[20,23] and Si NWs[24].

2 Computational Details

The single-particle electronic energies and wave functions are calculated using the plane-wave empirical pseudopotential method[25] and our recently derived and well-tested ZnO pseudopotentials[20]. The Hamiltonian for the single-particle states has the form

$$\hat{\mathrm{H}} = -\frac{1}{2}\nabla^2 + \sum_{n\alpha}[v_\alpha(\vec{r}-\vec{R}_{\alpha n}) + \hat{\mathrm{v}}_\alpha^{SO}], \qquad (1)$$

where n is an atomic index, α specifies the atom type and $\hat{\mathrm{v}}_\alpha^{SO}$ is the non-local spin-orbit operator. The screened atomic pseudopotentials v_α (with α = Zn,O) are centered at each atomic position and their superposition generates the crystal potential. $v_\alpha(\vec{r}-\vec{R}_{\alpha n})$ and $\hat{\mathrm{v}}_\alpha^{SO}$ are fitted to accurately reproduce

† Electronic Supplementary Information (ESI) available: Convergence test results.

[a] *Materials Science Department, University of Patras, 26504 Patras, Greece*
[b] *Institut für Physikalische Chemie, Universität Hamburg, Grindelallee 117, 20146 Hamburg, Germany*
* Corresponding author: bask@upatras.gr
‡ Corresponding author: gabriel.bester@uni-hamburg.de

well-known properties of bulk ZnO (e.g., band gap, critical energy levels, effective masses, and spin-orbit splittings), and the parameters are given in Ref. 20. This approach naturally includes the effects of multiband coupling, multivalley coupling, and spin-orbit interaction.

The ZnO NWs are constructed with a cross section as circular as possible, considering the atomistic nature of the structure. The supercells are extended and periodically repeated along the [0001] crystallographic direction, while the lateral surface of the NWs is well passivated by an artificial ligand with the same crystal structure and lattice parameters as ZnO and a higher band gap. Since there is no mismatch between the NW and the passivating material the electric field induced by piezoelectric effects can be safely neglected. The contribution of spontaneous polarization to the internal field is expected not to be significant since the polar direction of the NW coincides with the infinite growth direction. It has been demonstrated by large scale DFT calculations[26] that the internal field even in a polar quasi-one-dimensional nanorod (NR) does not depend strongly on the spontaneous polarization of the underlying lattice. This type of surface passivation has been practiced successfully previously for this material system[20,27,28], and very recently in Si NWs[24]. It should be noted here that the nature of the surface passivation and morphology may play an important role in the determination of the electronic and optical properties of semiconductor NWs, especially with smaller sizes. However, in our calculations, the emphasis is put on the size effects rather than the surface effects.

The many-body excitonic properties are calculated via configuration interaction (CI)[21]. The excitonic wave functions are expanded in terms of single-substitution Slater determinants constructed from the single-particle wave functions of electrons and holes. The corresponding many-body Hamiltonian is solved either in the framework of the single configuration (SC) approximation or in the CI scheme. At the SC level, the intraconfiguration Coulomb and exchange matrix elements are fully included, but the interaction between different configurations is neglected[21]. Consequently, the correlation effects at this level of theory are willingly not accounted for. The interconfiguration coupling is fully included in the CI scheme[21]. To capture the electron-hole interaction of excitons, the NWs are periodically expanded along the growth direction with a length of ∼4.164 nm, which is around three times the exciton Bohr radius in bulk ZnO (∼1.4 nm). The Coulomb and exchange integrals are screened by the position-dependent and size-dependent screening function proposed by Resta[29], which gives a physically smooth transition from short range (unscreened) to long range (screened)[21,24]. According to the results of the convergence test (see the supplementary materials), we include in the CI treatment eighteen states from the valence band and five states from the conduction band (not counting the spin degree of freedom), which ensures that the conduction band and valence band states are in a similar energy window. The optical dipole matrix elements are calculated within the dipole approximation, and the oscillator strength was calculated using Fermi's golden rule. A review of this method can be found in Ref. 30. It should be noted that our calculations are focused on the near-band-edge low energy excitonic states which are dominantly originated from the transistions at the Γ-point of the Brillouin zone. The band dispersion along the growth direction of the NWs is expected to have only very marginal influence on the results presented herein.

3 Numerical results and discussion

3.1 Electronic properties of ZnO nanowires

In an attempt to determine the electronic properties of ZnO NWs in both the intermediate and the weak confinement regimes, we consider five different ZnO NWs with diameters D = 2, 3, 4, 5, 6 nm. The fast oscillating atomic wave functions are projected onto bulk ZnO Bloch states, which enables us to visualize the envelope functions and quantify the Bloch function parentage of each NW state (i.e., to identify the contribution from each bulk Bloch state) [Ref. 20]. The envelope functions and Bloch function characters obtained from the projection for the first electron and first four hole states are presented in Fig. 1. We use the notation ω to characterize the symmetry of the envelope functions, where ω gives the number of nodes encountered when the envelope function is projected on a plane which contains both the growth direction vector and the center of the NW. The possible values of ω can be S, P and so forth, where S represents the an envelope function without node, P with one node, etc.. The results for the first four electron and first four hole states are presented in Table 1.

Table 1 Orbital character of the first four electron and hole envelope functions in ZnO NWs of various diameters (in unit of nm). The superscript (A,B,C) indicates the Bloch function parentage of the corresponding hole state obtained from Fig. 1.

Diameter	e_0	e_1	e_2	e_3	h_0	h_1	h_2	h_3
2	S	S	S	P	S^C	$P^{A,B}$	S^A	S^B
3	S	S	S	P	S^C	$P^{A,B}$	S^A	S^B
4	S	P	P	S	$P^{A,B}$	S^C	S^A	S^B
5	S	P	P	S	$P^{A,B}$	S^A	S^B	S^C
6	S	P	P	P	$P^{A,B}$	S^A	S^B	S^C

It is found that the lowest unoccupied molecular orbital (LUMO) state exhibits an S-like envelope function, derived purely from the lowest bulk conduction band, irrespectively of the variation of the level of quantum confinement. The fol-

lowing two electron states ($e_{1,2}$) appear to be energetically degenerate (see Fig. 2(a)), switching from an *S*-type to a *P*-type envelope function at a diameter around 3 nm. Furthermore, a *P*-like envelope function is more preferable for electron states $e_{1,2,3}$ in the presence of very weak quantum confinement effects (i.e., D = 6 nm $\approx 4.3a_B$, where $a_B = 1.4$ nm is the exciton Bohr radius of bulk ZnO).

Concerning the hole states, Fig. 1 and Table. 1 show that the wave functions with dominant single-band character (either A-, B-, or C-band) have *S*-type envelope functions, while the ones with an even mixing of bulk Bloch A- and B-bands have *P*-type envelope functions. The S^A and S^B states are energetically close to each other, whereas they are considerably separated from the S^C states (see Fig. 2(b)). This is a consequence of the nature of the topmost three valence bands in bulk ZnO, where the A- and B-bands are very close to each other, being energetically separated from the C-band. The S^C states exhibit a weaker diameter dependence than the S^A and S^B states (see Fig. 2(b)). Consequently, the A- and B-band states rise above the C-band states at the critical diameters $D_c^{A/C}$ and $D_c^{B/C}$, respectively, and become energetically more favorable, reproducing the usual electronic structure encountered in bulk ZnO. The critical values are $D_c^{A/C} = 4.2$ nm and $D_c^{B/C} = 4.6$ nm, respectively (see Fig. 2(b)). The $P^{A,B}$ states are energetically very close to the S^A and S^B states. The S^C states become the highest occupied molecular orbital (HOMO) states for diameter smaller than a critical value $D_c^{S/P} = 3.8$ nm (see Fig. 2(b)). These $P^{A,B}$ states are energetically more sensitive to the NW diameter, crossing over the S^C states at $D = D_c^{S/P}$ and becoming the HOMO states for $D > D_c^{S/P}$. This diameter dependent change in HOMO state from a conventional electronic state (e.g., with S-type envelope) to an unconventional state (e.g., with P-type envelope) has also been found previously in colloidal ZnO QDs[20] and very recently in GaN NWs[31], and is being attributed to the nontrivial interplay between symmetry mixing, spin-orbit coupling, and quantum confinement effects on the valence band electronic structure.

3.2 Optical properties of ZnO nanowires

First, we present the optical band gap of ZnO NWs for various diameters, which correspond to the intermediate or weak confinement regime (see Fig. 2(c)). The calculations are performed at three levels of theory, i.e., single-particle (SP) level, SC level, and CI level. Expectedly, the band gap appears to be a decreasing function of the NW diameter at all the three levels (see Fig. 2(c)). The size-dependent gaps are best fitted according to

$$\begin{aligned} E_g^{SP} &= E_g^{bulk} + \alpha/D^{\beta}, \\ E_g^{Op,SC} &= E_g^{bulk,op} + \alpha'/D^{\beta'}, \\ E_g^{Op,CI} &= E_g^{bulk,op} + \alpha''/D^{\beta''}, \end{aligned} \tag{2}$$

where E_g^{SP}, $E_g^{Op,SC}$, $E_g^{Op,CI}$ are the calculated single-particle gaps, optical band gaps at the SC level, optical band gaps at the CI level, respectively. $E_g^{bulk} = 3.445$ eV [Ref. 27] is the fundamental band gap of bulk ZnO, and $E_g^{bulk,op} = 3.385$ eV is the bulk optical gap. The respective values of the fitting parameters α, β, α', β', α'', β'' are 1.26, 1.33, 1.11, 1.5, 0.99, 1.54, where α, α' and α'' are in unit of eV·nm, while β, β' and β'' are dimensionless quantities. It is found that the diameter-dependent optical band gap of ZnO NWs (at the CI level), in the presence of quantum confinement effects, scales as $\sim 1/D^{1.54}$, rather than $\sim 1/D$ as predicted by the effective mass approximation[32]. The difference between the single-particle gap and the optical band gap at the CI level gives an exciton binding energy (in meV) which is best fitted by:

$$E_b^X = E_b^{bulk,X} + 310/D^{0.97}, \tag{3}$$

where $E_b^{bulk,X} = 60$ meV is the well-known exciton binding energy of bulk ZnO at room temperature. As expected from the quantum confinement effects, the exciton binding energy is significantly enhanced in ZnO NWs in comparison to bulk ZnO ($\sim$ 60 meV at room temperature), giving 111.25 meV at D = 6 nm, 140.99 meV at D = 4 nm and 218.78 meV at D = 2 nm, respectively.

The redshift of the emission spectra with respect to absorption spectra is known as the Stokes shift. It has two possible contributions[33]: (i) a purely electronic shift due to the splitting of exciton states into "bright" and "dark" states, which is usually called as *electronic Stokes shift*, and (ii) vibrational (phonon) relaxation due to movement of nuclei to new equilibrium positions in the excited state, which is called as *vibrational Stokes shift*. In general, the vibrational part is very difficult to model[33] since it requires excited state geometry optimization. Moreover, it has been well justified[34,35] that the Stokes shift in III-V and II-VI semiconductor nanostructures is mainly attributed to the (i) contribution. Therefore, in our calculations, the emphasis is put on the *electronic Stokes shift* which for brevity is called as Stokes shift. Its dependence on the NW diameter is shown in Fig. 2(d). The results are obtained at two levels of theory: at SC level and at CI level. It is found that the Stokes shift is a *non-monotonic* function of the diameter at both levels, having a maximum at a critical diameter value D_c. This critical values appear to be significantly different at both levels of theory, with $D_c^{SC} \approx 5$ nm at SC level, and it is $D_c^{CI} \approx 3$ nm at CI level. To understand this behaviour,

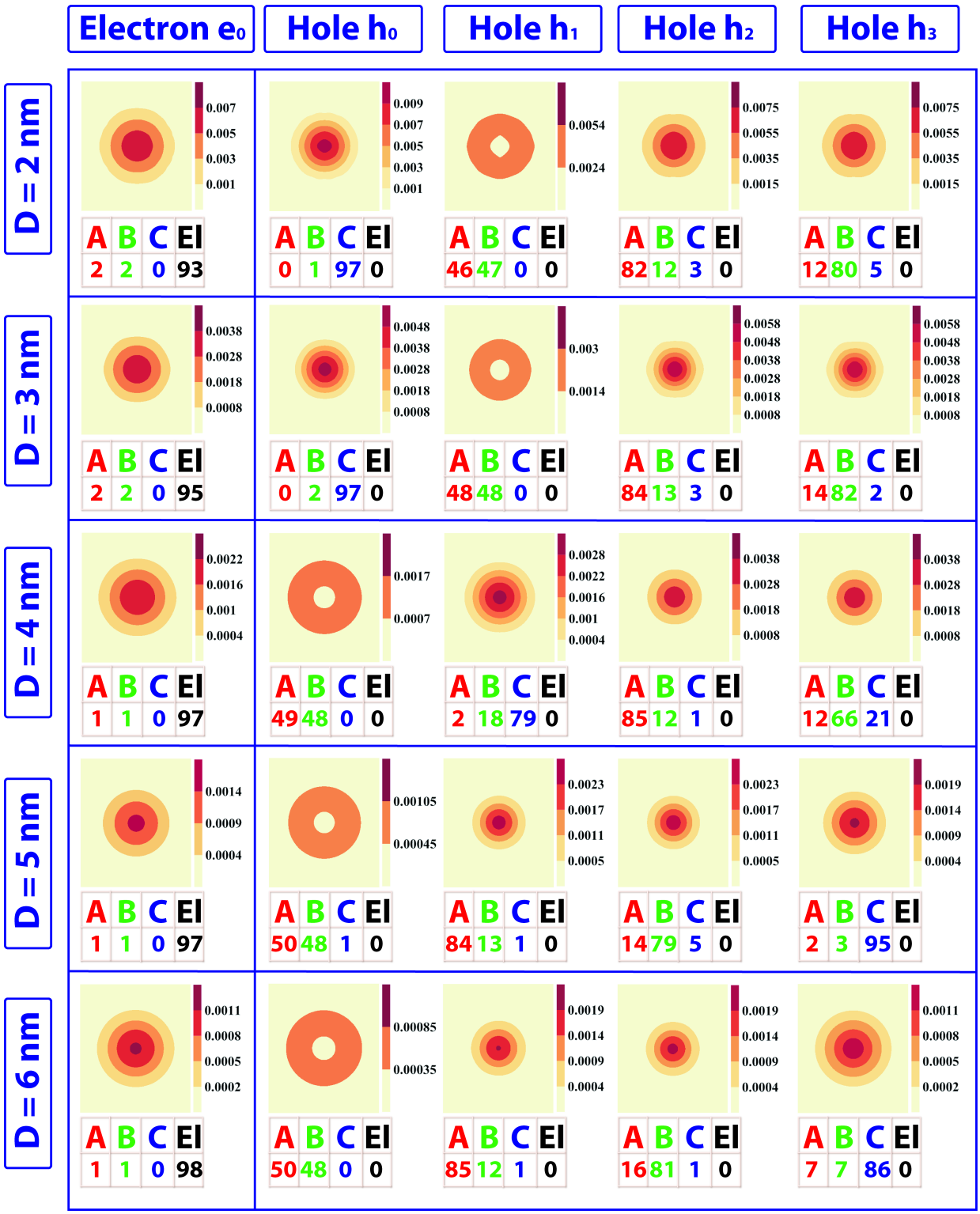

Fig. 1 Contour plot of the square of the envelope functions (perpendicular to the NW growth direction), extracted from our atomistic wave functions, for the first electron and first four hole states for various ZnO NWs. The parentage of each atomic NW wave function from the topmost three bulk valence band states (labeled as A, B and C) and the lowest bulk conduction band state (labeled as El) is tabulated under each plot in percentage.

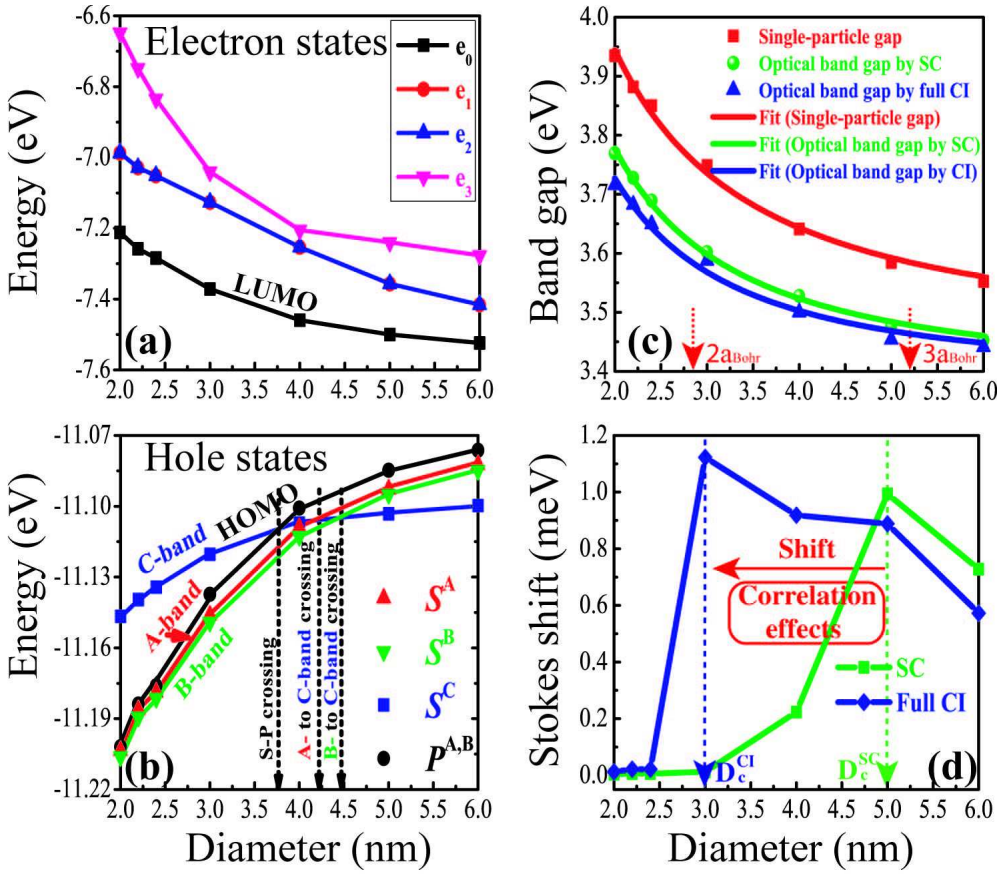

Fig. 2 (Color online) Single-particle electron states (a), hole states (b), (c) single-particle gap (red solid squares), optical band gap at SC level (green filled spheres) and optical band gap at the CI level (blue regular triangles), Stokes shift (d), as a function of the NW diameter. In figure (b), the lines connect states of the same symmetry ω. The red, green, blue, and black lines connect states with dominant A-band, B-band, C-band, and an even mixing of A- and B-bands parentage, respectively. In figure (c), each solid line represents a fit according to Eq. (2).

we take our smallest and largest NWs as examples and present the corresponding near-band-edge exciton pictures in the last column of Fig. 3. For $D < D_c$ (top panels in Fig. 3), the lowest and first bright exciton states belong to C-exciton at both SC and CI levels (the results at SC level are not shown), being contributed nearly purely (or dominantly) from the configuration where the hole state has an S-type envelope function and derives from bulk Bloch C-band (S^C state). However, for $D \geq D_c$, the two exciton states responsible for the Stokes shift switch to the A-exciton, deriving mainly from the configuration where the hole state has an S-type envelope function and a dominant bulk Bloch A-band parentage. This diameter-dependent C-exciton to A-exciton transition is responsible for the *non-monotonic* behaviour in Stokes shift.

We find from Fig. 3 that the formation of the optically dark and bright states is due to the electron-hole exchange interaction (see the last two columns). The C-exciton consists of one optically dark state and three optically bright states (see the upper panel of Fig. 3). The dark state is spin-forbidden and lower in energy. The lowest two bright exciton states are energetically very close to the dark state (i.e., $\sim$0.013 meV for D = 2 nm (by CI), see Fig. 2(d)), being doubly degenerate (with a very small splitting of 0.4 μeV (by CI)) and weakly polarized (with low intensity) along the in-plane direction. The third bright state is energetically far away (i.e., $\sim$4.01 meV (by CI) to the lowest dark state for D = 2 nm) and is singly degenerate with strong out-of-plane polarization (with high intensity). Concerning the A-exciton (see the lower panel of Fig. 3), it consists of two optically dark and two optically bright states. The dark states appear to be degenerate and present the ground state. The two bright exciton states are nearly degenerate with a small splitting of up to 58.25 μeV, being significantly separated from their dark counterparts (e.g., $\sim$ 0.573 meV for D = 6 nm). These results are in full agreement with the symmetry analysis developed by Hopfield[36]. The Stokes shift originating from different types of exciton is found to ex-

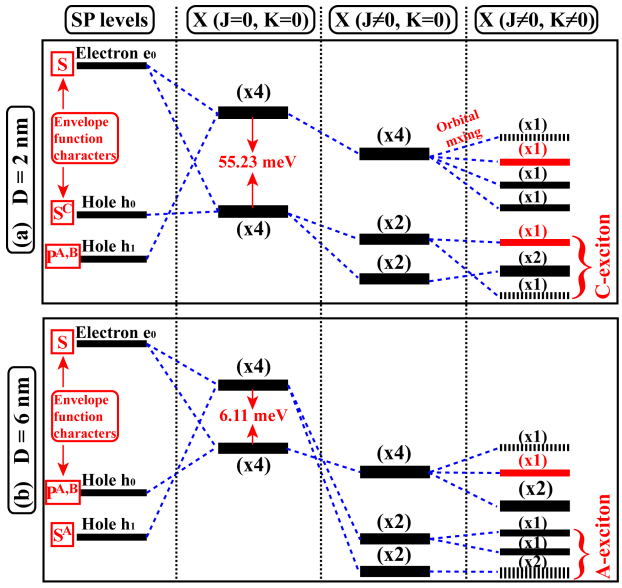

Fig. 3 Schematic picture of the evolution of the exciton states in ZnO NWs of two different diameters. From the left to the right columns are the single-particle states (column (i)), energy of the uncoupled electron-hole pairs (column (ii)), excitonic states obtained via CI including the Coulomb interaction but neglecting the exchange interaction (column (iii)), final result for the excitonic states including Coulomb, exchange and correlation effects (column (iv)). The numbers in parenthesis indicate the degeneracy of each level. The dark-exciton states, bright-exciton states with in-plane polarization, bright exciton states with out-of-plane polarization are shown in dashed black, solid black and solid red lines, respectively. For columns (ii)-(iv), the lowest total energy is placed at the bottom.

hibit a different diameter-dependence. As shown in Fig. 2(d), the Stokes shift derived from C-exciton states is quantitatively much smaller and it increases slightly with increasing diameter. Conversely, the one derived from A-exciton states turns out to be quantitatively much larger and it decreases significantly with respect to the increase in the diameter.

As mentioned previously, the S^A state rises over the S^C state and becomes energetically more favourable for $D > D_c^{A/C} = 4.2$ nm. Therefore, one might expect that the transition between the near-band-edge C-excition (electron-S—hole-S^C) and A-exciton (electron-S—hole-S^A) takes place around the critical value (≈ 4.2 nm). This is indeed the case if correlation effects are neglected. The maximum of the Stokes shift appears at a critical diameter $D_c^{SC} \approx 5$ nm, as shown by the SC results (see Fig. 2(d)). However, when the correlation effects are fully considered (see the CI results), the critical value at which the transition occurs shifts to a significantly smaller diameter value (e.g., $D_c^{CI} \approx 3$ nm). This nonmonotonic behaviour in Stokes shift has been found previously in several semiconductor nanostructures, e.g., CdSe NRs [Ref. 37], ZnO NRs [Ref. 27], ZnO QDs under pressure [Ref. 23]. A larger Stokes shift means a smaller overlap area between absorption and emission spectra, which is desirable in applications such as light-emitting diodes, where reabsorption reduces the total efficiency[37]. The transition between different types of excitons have recently been found in GaAs/AlGaAs QDs by applying elastic stress[38], which is believed to have potential application in quantum technologies.

We also find that the exciton nearly purely derived from a configuration (e,h) where the electron has an S-type envelope function (in LUMO) and the hole has a P-type envelope function does not exhibit the orbitally forbidden, dark ground state (see the lower panel). The exciton ground state appears to be orbitally allowed but spin-forbidden, derived from electron (in LUMO) and hole (in HOMO-1) with both S-type envelope functions, similar to the case of small diameter NWs (see the upper panel of Fig. 3). After the detailed analysis of the evaluation of the band-edge exciton states, (see Fig. 3) through the stepwise incorporation of Coulomb and exchange interactions, we find that two combined effects are responsible for this phenomenon:

(i) Increasing the diameter leads to a significant decrease in the energy difference between the two four-fold uncoupled states (see the second column of Fig. 3), e.g., the energy difference is 55.23 meV for D = 2 nm, while it is only 6.11 meV for D = 6 nm;

(ii) The Coulomb interaction is more pronounced for the configuration with both electron and hole having the same envelope function characters (both S-type) than that with electron and hole having different characters (electron: S-type, and hole: P-type), irrespective of the NW diameter. For example, for D = 2 nm, the Coulomb interaction experienced by the configuration (e_0,h_0) (e_0-S-h_0-S) is around 218.8 meV, while it is around 213.7 meV for the configuration (e_0,h_1) (e_0-S-h_1-P). These two values appear to be 106.6 meV (configuration (e_0,h_0), (e_0-S-h_1-P)) and 117.9 meV (configuration (e_0,h_1), (e_0-S-h_1-S)), for D = 6 nm.

This conventional optics from unconventional electronics has also been found previously in ZnO colloidal QDs[20]. Compared to the Coulomb interaction, the influence of the exchange interaction (fourth column of Fig. 3) has a significantly smaller magnitude (below 1 meV, depending on the NW diameter) but is important for the optical polarization properties.

Finally, we present in Fig. 4 the absorption spectrum at room temperature for various NW diameters. The calculations are performed in the CI scheme. A Gaussian broadening function is adopted with a broadening parameter of 1.2 meV. It is found that increasing the diameter leads to a redshift in the absorption spectrum. This redshift is more pronounced for narrow NWs (with small diameters). Decreasing the NW diameter results in a transition in the optical absorption polarization from an in-plane polarization ($\mathbf{E}\perp\vec{c}$) to an out-of-plane

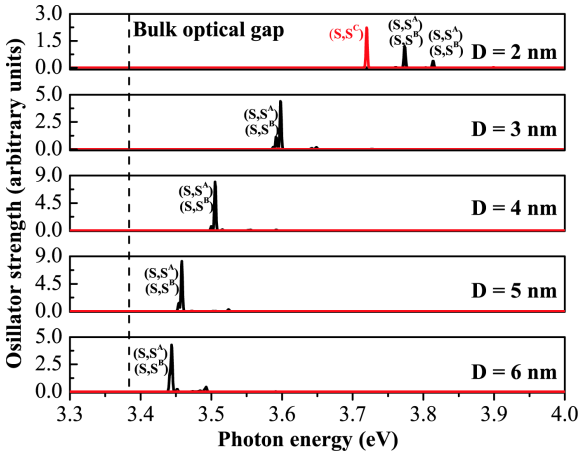

Fig. 4 Oscillator strength for the absorption $\langle 0|$ to $\langle X|$ in various ZnO NWs at room temperature obtained via CI. Absorptions polarized along the out-of-plane (c axis) and in-plane (perpendicular to the c-axis) directions are shown by red and black vertical lines, respectively. The symbols in parentheses indicate the dominant envelope function characters of the single-particle states (e,h) involved in the absorptions, and the parentage of the corresponding hole state is given as superscript.

polarization ($\mathbf{E}\|\vec{c}$) at a diameter of around 3 nm. This transition between *usual* α-absorption ($\mathbf{E}\perp\vec{c}$) and *unusual* σ and π absorptions ($\mathbf{E}\|\vec{c}$) has also been found previously in ZnO QDs under hydrostatic pressures[23] and ZnO NRs by changing the length-to-diameter aspect ratios[27]. Before the transition occurs (e.g., for $D\geq 3$ nm), the near-band-edge optical absorption is dominated by the A- and B-exciton absorptions, which can not be separately resolved experimentally[13]. However, after the transition takes place (e.g., for $D<3$ nm), the *unusual* C-exciton absorption (σ and π absorptions) becomes active. This type of absorption in ZnO NWs has been recently experimentally achieved by Jacopin *et al.*[13] using a thermal approach. The results we present here offer a new way (e.g., narrowing the NW diameter) to activate the C-exciton absorption in ZnO NWs, which should be very interesting for the design of future experiments in the realm of quantum technology[38].

4 Conclusions

In the present work, we have studied the electronic and optical properties of ZnO NWs as a function of the diameter. We find that the hole states with dominant single-band (bulk A-, B- or C-band) parentage exhibit S-type envelope functions, while the states with an even mixture of bulk Bloch A- and B-bands present P-type envelope functions. The A-band and B-band states are very close in energy and more sensitive to the NW diameter than the C-band states. Consequently, these states rise over the C-band states at a critical diameters (e.g., $D_c^{A/C}=4.2$ nm and $D_c^{B/C}=4.8$ nm) and become energetically more favourable, reproducing the usual electronic structure of bulk ZnO. Comparing to the C-band states, the states with an even mixture of bulk Bloch A- and B-bands parentage exhibit a stronger size-dependence, causing a drastic change in the envelope function character of the highest occupied molecular orbital (HOMO) state from a *conventional S*-like character to an *unconventional P*-like character at diameter around 3.8 nm. The lowest unoccupied molecular orbital (LUMO) state always presents an S-type envelope function, irrespectively of the variation of the quantum confinement effects.

The optical band gap is a decreasing function of the NW diameter and scales as $\sim 1/D^{1.54}$, rather than $\sim 1/D$ as expected from effective mass theory. The exciton binding energy is calculated and the associated scaling law is provided. In contrast to monotonic behaviour in the optical band gap, the Stokes shift displays a non-monotonic function of the diameter, exhibiting a maximum at a critical diameter value around 3 nm. We explain this behaviour through the transition of the near-band-edge exciton from a usual C-exciton to an unusual A-exciton by varying the NW diameters. For NWs larger than the critical diameter, the near-band-edge optical absorption is dominated by the in-plane polarized A- and B-exciton absorptions. For NWs smaller than the critical diameter the out-of-plane polarized C-exciton absorption is dominant.

Acknowledgement

This research has been co-financed by the European Union (European Social Fund-ESF) and Greek national funds through the Operational Program "Education and Lifelong Learning" of the National Strategic Reference Framework (NSRF)-Research Funding Program: Thales, investing in knowledge society through the European Social Fund.

References

1 P. Yang, H. Yan, S. Mao, R. Russo, J. Johnson, R. Saykally, N. Morris, J. Pham, R. He and H.-J. Choi, *Adv. Funct. Mater.*, 2002, **12**, 323–331.
2 X.-Y. Liu, C.-X. Shan, S.-P. Wang, Z.-Z. Zhang and D.-Z. Shen, *Nanoscale*, 2012, **4**, 2843–2846.
3 C. Liu, J. Zapien, Y. Yao, X. Meng, C. Lee, S. Fan, Y. Lifshitz and S. Lee, *Adv. Mater.*, 2003, **15**, 838–841.
4 Z. Fan, P.-C. Chang, J. G. Lu, E. C. Walter, R. M. Penner, C.-H. Lin and H. P. Lee, *Appl. Phys. Lett.*, 2004, **85**, 6128–6130.
5 Y. T. Lee, S. R. Ali Raza, P. J. Jeon, R. Ha, H.-J. Choi and S. Im, *Nanoscale*, 2013, **5**, 4181–4185.
6 H. Kind, H. Yan, B. Messer, M. Law and P. Yang, *Adv. Mater.*, 2002, **14**, 158–160.
7 K. Keem, H. Kim, G.-T. Kim, J. S. Lee, B. Min, K. Cho, M.-Y. Sung and S. Kim, *Appl. Phys. Lett.*, 2004, **84**, 4376–4378.
8 Q. Wan, Q. H. Li, Y. J. Chen, T. H. Wang, X. L. He, J. P. Li and C. L. Lin, *Appl. Phys. Lett.*, 2004, **84**, 3654–3656.
9 C. Baratto, S. Todros, G. Faglia, E. Comini, G. Sberveglieri, S. Lettieri,

L. Santamaria and P. Maddalena, *Sens. Actuator B-Chem.*, 2009, **140**, 461 – 466.
10 Z. L. Wang and J. Song, *Science*, 2006, **312**, 242–246.
11 G. Zhu, R. Yang, S. Wang and Z. L. Wang, *Nano Lett.*, 2010, **10**, 3151–3155.
12 Q. Wan, C. L. Lin, X. B. Yu and T. H. Wang, *Appl. Phys. Lett.*, 2004, **84**, 124–126.
13 G. Jacopin, L. Rigutti, A. Bugallo, F. Julien, C. Baratto, E. Comini, M. Ferroni and M. Tchernycheva, *Nanoscale Res. Lett.*, 2011, **6**, 501.
14 F.-H. Chu, C.-W. Huang, C.-L. Hsin, C.-W. Wang, S.-Y. Yu, P.-H. Yeh and W.-W. Wu, *Nanoscale*, 2012, **4**, 1471–1475.
15 Y. Gu, I. L. Kuskovsky, M. Yin, S. O'Brien and G. F. Neumark, *Appl. Phys. Lett.*, 2004, **85**, 3833–3835.
16 M. Şahin, S. Nizamoglu, A. E. Kavruk and H. V. Demir, *J. Appl. Phys.*, 2009, **106**, 043704.
17 A. W. Long and B. M. Wong, *AIP Adv.*, 2012, **2**, 032173.
18 H. J. Xiang, J. Yang, J. G. Hou and Q. Zhu, *Appl. Phys. Lett.*, 2006, **89**, 223111.
19 Z. Xu, Q.-R. Zheng and G. Su, *Phys. Rev. B*, 2012, **85**, 075402.
20 S. Baskoutas and G. Bester, *J. Phys. Chem. C*, 2010, **114**, 9301.
21 A. Franceschetti, H. Fu, L. W. Wang and A. Zunger, *Phys. Rev. B*, 1999, **60**, 1819–1829.
22 M. Califano, A. Zunger and A. Franceschetti, *Nano Lett.*, 2004, **4**, 525–531.
23 Z. Zeng, C. S. Garoufalis, S. Baskoutas and G. Bester, *Phys. Rev. B*, 2013, **87**, 125302.
24 L. Zhang, J.-W. Luo, A. Franceschetti and A. Zunger, *Phys. Rev. B*, 2011, **84**, 075404.
25 L.-W. Wang and A. Zunger, *J. Chem. Phys.*, 1994, **100**, 2394–2397.
26 P. W. Avraam, N. D. M. Hine, P. Tangney and P. D. Haynes, *Phys. Rev. B*, 2011, **83**, 241402.
27 S. Baskoutas and G. Bester, *J. Phys. Chem. C*, 2011, **115**, 15862–15867.
28 M. Califano, G. Bester and A. Zunger, *Nano Lett.*, 2003, **3**, 1197–1202.
29 R. Resta, *Phys. Rev. B*, 1977, **16**, 2717.
30 G. Bester, *J. Phys: Conden. Matter*, 2009, **21**, 023202.
31 A. Molina-Sanchez, A. Garcia-Cristobal and G. Bester, *Phys. Rev. B*, 2012, **86**, 205430.
32 L. E. Brus, *J. Chem. Phys.*, 1984, **80**, 4403–4409.
33 B. S. Kim, M. A. Islam, L. E. Brus and I. P. Herman, *J. Appl. Phys.*, 2001, **89**, year.
34 A. Bagga, P. K. Chattopadhyay and S. Ghosh, *Phys. Rev. B*, 2006, **74**, 035341.
35 D. O. Demchenko and L.-W. Wang, *Phys. Rev. B*, 2006, **73**, 155326.
36 J. Hopfield, *J. Phys. Chem. Solids*, 1960, **15**, 97 – 107.
37 J. Hu, L.-S. Li, W. Yang, L. Manna, L.-W. Wang and A. P. Alivisatos, *Science*, 2001, **292**, 2060–2063.
38 Y. H. Huo, B. J. Witek, S. Kumar, J. R. Cardenas, J. X. Zhang, N. Akopian, R. Singh, E. Zallo, R. Grifone, D. Kriegner, R. Trotta, F. Ding, J. Stangl, V. Zwiller, G. Bester, A. Rastelli and O. G. Schmidt, *Nat. Phys.*, 2014, **10**, 46 – 51.